World Scientific
www.worldscientific.com

Point-contact Andreev reflection spectroscopy on Bi$_2$Se$_3$ single crystals

C. R. Granstrom[*], I. Fridman[*], H.-C. Lei[†], C. Petrovic[†] and J. Y. T. Wei[*,‡,§]

[*]*Department of Physics, University of Toronto,*
60 St. George St., Toronto M5S1A7, Canada
[†]*Condensed Matter Physics & Materials Science Department,*
Brookhaven National Laboratory, NY 11973, USA
[‡]*Canadian Institute for Advanced Research, Toronto M5G1Z8, Canada*
[§]*wei@physics.utoronto.ca*

To study how Andreev reflection (AR) occurs between a superconductor and a three-dimensional topological insulator (TI), we use superconducting Nb tips to perform point-contact AR spectroscopy at 4.2 K on as-grown single crystals of Bi$_2$Se$_3$. Scanning tunneling spectroscopy and scanning tunneling microscopy are also used to characterize the superconducting tip and both the doping level and surface condition of the TI sample. The point-contact measurements show clear spectral signatures of AR, as well as a depression of zero-bias conductance with decreasing junction impedance. The latter observation can be attributed to interfacial Rashba spin-orbit coupling, and the presence of bulk bands at the Fermi level in our samples suggests that bulk states of Bi$_2$Se$_3$ are involved in the observed AR.

Keywords: Andreev reflection; topological insulator; superconductor.

PACS numbers: 74.45.+c, 73.20.At, 73.63.Rt

1. Introduction

Three-dimensional topological insulators (TIs) are a novel class of materials where strong spin-orbit coupling causes bulk band inversion, resulting in surface states with Dirac dispersion and helical spin polarization that are topologically-protected against back-scattering.[1,2] Andreev reflection (AR) is the process that converts a normal-current to a super-current across a metal/superconductor interface. For conventional metals, AR has been extensively studied and is quite well understood.[3–7] For three-dimensional TIs, however, there have been no explicit experimental or theoretical studies of AR. Generally speaking, AR is known to be affected by Fermi-wave vector mismatch,[4] spin polarization,[8–12] Rashba spin-orbit coupling (RSOC),[13–17] and Dirac dispersion.[18] Considering the unique attributes of

three-dimensional TIs, it is therefore interesting to examine whether and how AR occurs onto topological surface states (TSS).

The preferred method for measuring AR is to place a sharp tip in ballistic contact with a sample, in a technique called point-contact AR spectroscopy (PCARS), which has the following advantages. First, the small size of the tip/sample junction ensures local voltage drop. Second, spectral analysis is amenable to the Blonder–Tinkham–Klapwijk (BTK) theory, which was specifically developed for 1D micro-constrictions.[3] Third, the point-contact geometry minimizes local attenuation of the pair potential in the superconducting electrode,[7,19] thus simplifying spectral analysis. Fourth, the tip can be cleaned by *in situ* field emission. Lastly, many junctions can be made in a single experiment, to check for spectral reproducibility.

In this study, we perform PCARS on as-grown Bi_2Se_3 single crystals using superconducting Nb tips. Scanning tunneling spectroscopy (STS) and scanning tunneling microscopy (STM) are also used to characterize the superconducting tip and both the doping level and surface condition of the TI sample. These tunneling measurements show that our tip and sample are clean, and that the Fermi level of our as-grown Bi_2Se_3 crystals is in the bulk conduction band (BCB). The point-contact measurements show clear spectral signatures of AR, along with an asymmetric conductance background that can be attributed to the band structure of Bi_2Se_3. We also observe a depression of zero-bias conductance with decreasing junction impedance, which can be attributed to interfacial RSOC. The presence of bulk bands at the Fermi level in our samples suggests that bulk states of Bi_2Se_3 are involved in the observed AR.

2. Experiment

The Bi_2Se_3 single crystals used in this study were grown by the flux method. The as-grown crystals were *n*-type doped as a result of naturally occurring defects, which are common in the bismuth chalcogenides. PCARS and STS measurements were made using a home-built STM at 4.2 K in a ^{4}He dipper probe. For PCARS, differential conductance versus bias voltage was measured using a four-terminal geometry with an AC resistance bridge. For STS, standard two-point AC lock-in technique was used. For PCARS, the STM approach method was used to gently bring the tip and sample into contact without crashes. Namely, a piezo stepper motor with a ~ 10 nm step size was used to move the tip in to tunneling range of the sample. The STM feedback was then disengaged, the four-terminal wiring engaged, and the tip gently brought into contact with the sample using the STM piezo. Nb tips of 99.9% purity were cut and cleaned *in situ* through high-voltage field emission on a Ag film. The Bi_2Se_3 crystals were cleaved either in air or *in situ* in 99.99% pure ^{4}He exchange gas. To check for spectral reproducibility, numerous Nb–Bi_2Se_3 junctions were made on several crystals. Measurement accuracies of both the STS and PCARS setups were validated using Nb tips on Ag films and Au foil, respectively.

3. Results

Figure 1 shows typical PCARS data for a Nb tip on a Bi$_2$Se$_3$ crystal cleaved in air. The dI/dV conductance spectra for various junction impedances are plotted versus sample-to-tip bias voltage V, and staggered vertically for clarity. The spectrum for the highest junction impedance (80 ohms, bottom trace) shows a broad hump within ± 10 mV, indicating an AR conductance enhancement of $\sim 10\%$.[a] As the tip is pushed into the sample, thereby decreasing the junction impedance to 5 ohms (top trace), the zero-bias conductance dips and two peaks emerge. The peak separation is ~ 4 mV, which can be compared with our STS data for a Nb tip on a Ag film, shown in Fig. 2(a). Although the superconducting gap of Nb is ~ 1.5 meV at 0 K, spectral smearing due to finite quasiparticle lifetime and broadening of the Fermi–Dirac function at 4.2 K causes the coherence peaks in STS data to shift to $\sim \pm 2.5$ mV. The clear AR peaks we observed in Fig. 1 are consistent with a clean tip as evidence by the STS data in Fig. 2(a), and with a clean sample surface as shown by the atomically-resolved STM image in the inset of Fig. 2(b).

In the standard BTK model, AR is not expected to produce any spectral asymmetry about zero bias. However, our PCARS data (Fig. 1) appear to be asymmetric, both in the AR peak heights and in the background conductance. To understand the origin of the peak-height asymmetry, we normalized each spectrum by dividing out the background conductance, after interpolating it from outside the ± 15 mV range. This normalization procedure has the effect of symmetrizing each spectrum (not shown), indicating that the peak-height asymmetry is due to the spectral background and thus is not intrinsic to the AR. The asymmetric spectral background is also seen in our STS data for Bi$_2$Se$_3$ [Fig. 2(b)]. Its overall shape is consistent with previous STS data reported for Bi$_2$Se$_3$ single crystals,[20] and with density-of-states calculations.[21] A more detailed comparison of our STS data with these prior studies indicate that, in our as-grown Bi$_2$Se$_3$ crystals, the Fermi level is in the BCB and the Dirac point (E_D) is ~ 350 mV below the Fermi level, with no bulk bands lying at the same energy as E_D.[22]

Figure 3 shows PCARS data taken on a Bi$_2$Se$_3$ crystal that was cleaved *in situ* in 99.99% pure ^{4}He gas. In these spectra, as the junction impedance is decreased from 20 ohms to 10 ohms, a hump structure also splits into two peaks, but farther apart than the data for the air-cleaved crystal (Fig. 1). Additionally, the AR conductance enhancement here ($\sim 2\%$ for the bottom trace in Fig. 3) is weaker than for the air-cleaved crystal ($\sim 10\%$ for the bottom trace in Fig. 1). The differences between these two sets of data can be understood in terms of the "spreading" resistance resulting from the wiring configuration. Namely, unlike *ex situ* cleaved crystals where the sample leads are on the crystal surface, *in situ* cleaving requires the sample leads to be attached to the sides of the crystal, thus forcing the current

---

[a]This conductance enhancement is defined as the zero-bias height of the AR hump relative to above-gap conductance, after normalizing the entire spectrum by a spectral background that is interpolated from outside the ± 15 mV range.
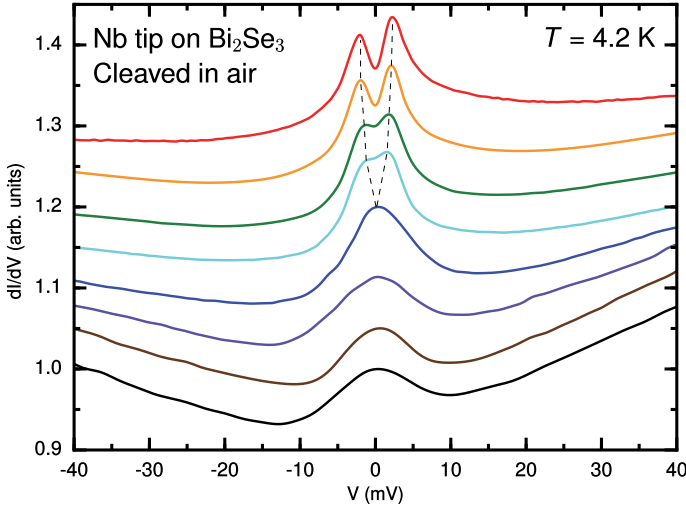
Fig. 1.   PCARS data taken at 4.2 K with a Nb tip on air-cleaved Bi_2Se_3 as the tip is pushed into the sample. As the junction impedance decreases from 80 ohms (bottom trace) to 5 ohms (top trace), the zero-bias conductance dips and two peaks emerge at ± 2 mV. Each trace is divided by its conductance at -40 mV and is shifted vertically for clarity.
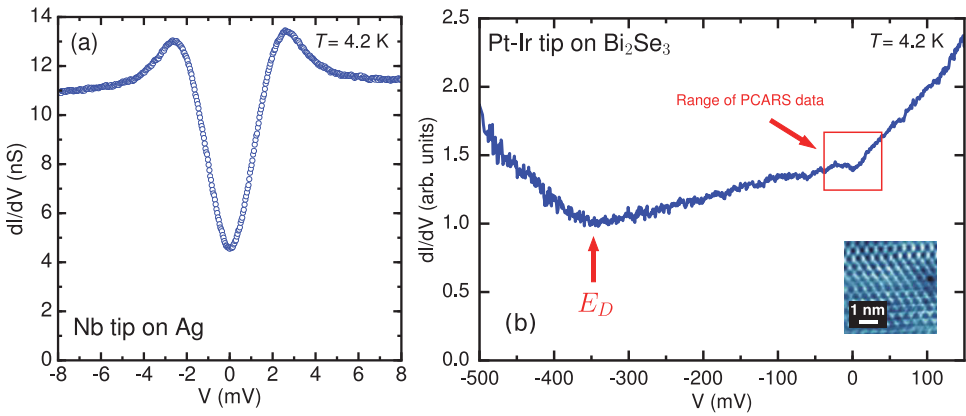

Fig. 2.   (a) STS data for a Nb tip on a Ag film at 4.2 K. The spectrum was taken with sample bias $V_s = -18$ mV and tunneling current $I_t = 0.2$ nA. (b) STS data taken on Bi_2Se_3 with a Pt–Ir tip at 4.2 K, using $V_s = -80$ mV and $I_t = 0.1$ nA. As described in the text, the Fermi level is in the BCB, and the Dirac point is at -350 mV. The inset shows an atomically-resolved STM image of a Bi_2Se_3 crystal with $V_s = -400$ mV and $I_t = 2$ nA.

to flow along the *c*-axis of the crystal. This is illustrated in the inset of Fig. 3. Since the *c*-axis resistivity of Bi_2Se_3 is ~ 15 times larger than its *ab*-plane resistivity,[23] the four-terminal resistance can be effectively "spread" outside the point-contact and into the sample. Such spreading resistance tends to lower and broaden the measured AR characteristics,[24,25] thus explaining the spectral differences between our
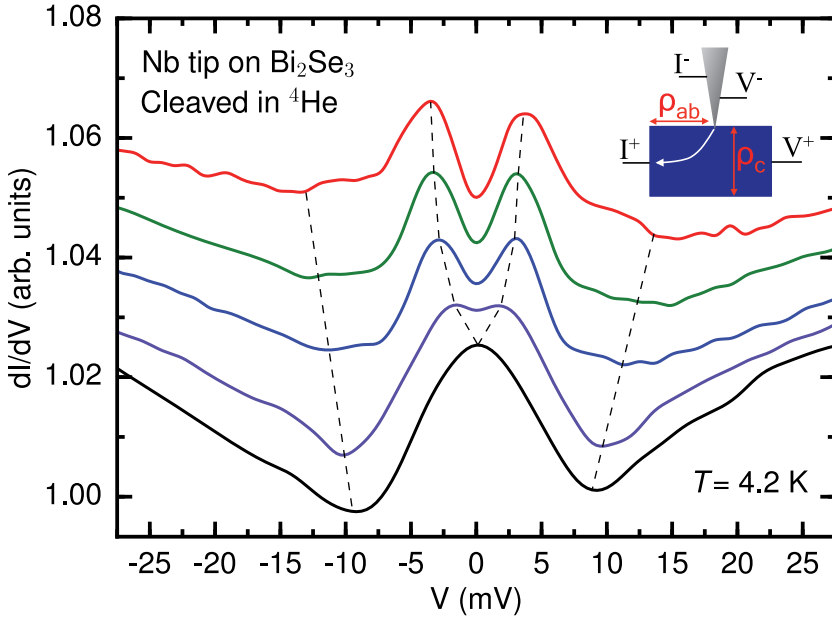
Fig. 3.   PCARS data taken at 4.2 K with a Nb tip on Bi$_2$Se$_3$ cleaved in 99.99% pure ^{4}He exchange gas, as the tip is pushed into the sample. As the junction impedance decreases from 20 ohms (bottom trace) to 10 ohms (top trace), a broad hump splits into two peaks separated by 7 mV. The AR conductance enhancement is weaker here than for Bi$_2$Se$_3$ cleaved in air. Also visible are dips that evolve into humps at ± 12 mV. Each trace is divided by its conductance at -25 mV and is shifted vertically for clarity. The inset shows the contact configuration required for *in situ* cleaving, whereby the current has to flow along the higher resistance *c*-axis.

^{4}He-cleaved and air-cleaved crystals. Here, it is worth noting a peculiar spectral feature in the ^{4}He-cleaved case, namely the dips that evolve into humps at $\sim\pm 12$ mV as junction impedance decreases. The origin of this feature is not yet known, but its apparent correlation with the AR peak splitting suggests that it is related to AR.

4. Discussion

In our PCARS data, the hump-to-peaks spectral evolution versus decreasing junction impedance may be attributed to interfacial RSOC. In a non-topological context, RSOC has already been shown to depress AR at low energies.[13–16] A mechanism that may enhance this AR depression is band bending, which would strengthen the RSOC by inducing an electric field at the interface. Band bending can occur at an interface between two materials whenever there is a large difference in their Fermi energies, such as between a metal and a semiconductor.[26] In our case of an interface between metallic Nb and semimetallic Bi$_2$Se$_3$, a decrease in the junction impedance could increase the band bending, thereby strengthening the field-induced RSOC to enhance the AR depression. It is worth noting that

Bi_2Se_3 is susceptible to band bending via surface adsorbates, as has been observed by ARPES[27–30] on samples deliberately exposed to water vapor.

It is likely that our PCARS data is influenced by topologically trivial bulk states present at the crystal surface, since our STS data indicate that the Fermi level crosses the BCB in our as-grown crystals. A natural question is, to what extent is the AR occurring onto the TSS? To answer this question, the dimensionality difference between the TSS and the bulk bands must be taken into account, as two- and three-dimensional extensions of the BTK theory have shown that AR is affected by Fermi-surface dimensionality.[31,32] Other likely important factors are the spin-momentum locking and Dirac dispersion of the TSS. For instance, the former factor may enhance AR via suppression of back-scattering. Further refinements of the BTK theory would be needed to elucidate this possibility.

5. Summary

In an effort to understand how AR occurs between a superconductor and a three-dimensional TI, we have performed PCARS using superconducting Nb tips on as-grown single crystals of Bi_2Se_3. STS and STM were also used to characterize the superconducting tip and both the doping level and surface condition of the TI sample. These tunneling measurements show that our tip and sample are clean, and that the Fermi level of our as-grown Bi_2Se_3 crystals is in the BCB. Our PCARS data show clear spectral signatures of AR, along with an asymmetric conductance background that can be attributed to the band structure of Bi_2Se_3. We also observe a depression of zero-bias conductance with decreasing junction impedance, which can be attributed to interfacial RSOC. The presence of bulk bands at the Fermi level indicates that both bulk and surface states are involved in the observed AR, with the dimensionality difference between these states determining their relative contributions to the AR. Other important factors to consider are the spin-momentum locking and Dirac dispersion of the TSS. Further measurements, along with refinements of the BTK theory taking into account the unique attributes of TIs, are necessary to clarify these issues.

References

1. M. Z. Hasan and C. L. Kane, *Rev. Mod. Phys.* **82**, 3045 (2010).
2. X.-L. Qi and S.-C. Zhang, *Rev. Mod. Phys.* **83**, 1057 (2011).
3. G. E. Blonder, M. Tinkham and T. M. Klapwijk, *Phys. Rev. B* **25**, 4515 (1982).
4. G. E. Blonder and M. Tinkham, *Phys. Rev. B* **27**, 112 (1983).
5. B. Pannetier and H. Courtois, *J. Low Temp. Phys.* **118**(5–6), 599 (2000).
6. T. Klapwijk, *J. Supercond.* **17**(5), 593 (2004).
7. D. Daghero and R. S. Gonnelli, *Supercond. Sci. Technol.* **23**(4), 043001 (2010).
8. M. J. M. de Jong and C. W. J. Beenakker, *Phys. Rev. Lett.* **74**, 1657 (1995).
9. R. J. Soulen *et al.*, *Science* **282**(5386), 85 (1998).
10. Y. Ji *et al.*, *Phys. Rev. Lett.* **86**, 5585 (2001).
11. I. Žutić, *J. Fabian and S. Das Sarma, Rev. Mod. Phys.* **76**, 323 (2004).

12. S. K. Upadhyay *et al.*, *Phys. Rev. Lett.* **81**, 3247 (1998).
13. T. Yokoyama, Y. Tanaka and J. Inoue, *Phys. Rev. B* **74**, 035318 (2006).
14. S. Wu and K. V. Samokhin, *Phys. Rev. B* **82**, 184501 (2010).
15. S. Wu and K. V. Samokhin, *Phys. Rev. B* **81**, 214506 (2010).
16. A. Kononov *et al.*, *JETP Lett.* **98**(7), 421 (2013).
17. P. Högl *et al.*, *Phys. Rev. Lett.* **115**, 116601 (2015).
18. C. W. J. Beenakker, *Phys. Rev. Lett.* **97**, 067007 (2006).
19. G. Deutscher, *Rev. Mod. Phys.* **77**, 109 (2005).
20. T. Hanaguri *et al.*, *Phys. Rev. B* **82**, 081305 (2010).
21. Y. Zhao *et al.*, *Nano Lett.* **11**(5), 2088 (2011), PMID: 21495641.
22. Y. Xia *et al.*, *Nat Phys.* **5**(6), 398 (2009).
23. W. H. Jiao *et al.*, *AIP Advances* **2**(2), 022148 (2012).
24. T. Y. Chen, S. X. Huang and C. L. Chien, *Phys. Rev. B* **81**, 214444 (2010).
25. B. Nadgorny, *Handbook of Spin Transport and Magnetism* (Taylor and Francis, New York, 2011).
26. H. Lüth, *Solid Surfaces, Interfaces, and Thin Films, Springer*, 5th edn. (Springer Berlin Heidelbug, Germany, 2010).
27. M. Bianchi *et al.*, *Nat Commun.* **1**, 128 (2010).
28. H. M. Benia *et al.*, *Phys. Rev. Lett.* **107**, 177602 (2011).
29. P. D. C. King *et al.*, *Phys. Rev. Lett.* **107**, 096802 (2011).
30. Z.-H. Zhu *et al.*, *Phys. Rev. Lett.* **107**, 186405 (2011).
31. D. Daghero *et al.*, *Rep. Prog. Phys.* **74**(12), 124509 (2011).
32. D. Daghero *et al.*, *Low Temp. Phys.* **39**(3), 199 (2013).